Textile fabric's in-plane water permeability determination during wicking

DOI: 10.35530/IT.075.05.20241

SOFIEN BENLTOUFA AYMAN ALFALEH

ABSTRACT – REZUMAT

Textile fabric's in-plane water permeability determination during wicking

Based on a mathematical formulation of the water flow for different wicking configurations (ascendant-horizontal and descendant), a combined ascendant, horizontal and descendant wicking experimental test was designed to provide detailed measurements of the pertinent wicking performance properties: capillary pressure and in-plane direction permeability. This method was proposed due to capillary flows found in standard vertical wicking tests as well as erroneous assumptions made in other wicking tests. The effective capillary radius was assumed to remain constant as the height of the liquid increases. This assumption would suggest that saturation, capillary pressure, and permeability are also constants. However, experiments show that these properties are only constants in the case of the descendant wicking when liquid front height is varied. The capillary pressure and permeability calculations were made using Darcy's law and the Lucas-Washburn equation as a function of the saturation level. In the combined wicking test, conducting a horizontal wicking test allows us to calculate the effective capillary radius of a fabric as the saturation rate was found to be constant, which in turn can be used to solve for capillary pressure. That capillary pressure can then be used in a descendant wicking test, where the liquid front flow and the saturation rate remain constant, and Darcy's law to solve for permeability. A series of experiments was conducted on cotton jersey knitting. The results showed that the ability to wick the water depends on pore size and porosity scales: macro and micropores. The in-plane water permeability was found to be directly related to the saturation rate.

Keywords: *capillary pressure, combined wicking, saturation rate, water permeability*

Determinarea permeabilității la apă în plan a materialului textil în timpul absorbției

Pe baza unei formule matematice a fluxului de apă pentru diferite configurații de absorbție (ascendentă-orizontală și descendentă), a fost conceput un test experimental combinat de absorbție ascendentă, orizontală și descendentă pentru a furniza determinări detaliate ale proprietăților de performanță a absorbției relevante: presiunea capilară și permeabilitatea direcției în plan. Această metodă a fost propusă din cauza fluxurilor capilare găsite în testele standard de absorbție verticală, precum și a presupunerilor eronate făcute în alte teste de absorbție. S-a presupus că raza capilară efectivă rămâne constantă pe măsură ce înălțimea lichidului crește. Această ipoteză ar sugera că saturația, presiunea capilară și permeabilitatea sunt, de asemenea, constante. Cu toate acestea, experimentele arată că aceste proprietăți sunt constante doar în cazul absorbției descendente atunci când înălțimea frontului lichid este variată. Calculele presiunii capilare și permeabilității au fost efectuate folosind legea lui Darcy și ecuația Lucas-Washburn în funcție de nivelul de saturație. În testul combinat de absorbție, efectuarea unui test de absorbție orizontală ne permite să calculăm raza capilară efectivă a unui material textil, deoarece s-a constatat că rata de saturație este constantă, și care, la rândul său, poate fi utilizată pentru a rezolva presiunea capilară. Această presiune capilară poate fi apoi utilizată într-un test de absorbție descendentă, în care fluxul frontal al lichidului și rata de saturație rămân constante, iar legea lui Darcy se aplică pentru permeabilitate. S-au efectuat o serie de experimente pe tricotul din bumbac. Rezultatele au arătat că această capacitate de a absorbi apa depinde de dimensiunea porilor și de gradele de porozitate: macro și micropori. S-a constatat că permeabilitatea la apă în plan este direct legată de rata de saturaţie.

Cuvinte-cheie*: presiune capilară, absorbție combinată, rata de saturație, permeabilitate la apă*

INTRODUCTION

The thermophysiological comfort afforded by textile fabrics, as a second skin, can be improved by understanding the liquid transport mechanism. During high activities or in hot atmosphere conditions, the body sweats. The excess of the accumulated liquid should be removed to the external environment atmosphere by evaporation [1–5] and wicking [6–8], especially for fabric surface not exposed to the external air.

Liquid transfer through textile fabrics was an attractive research area. The constituted yarns are the main ones responsible for the wicking action through the textile fabrics [9, 10]. Yarns were handled either as a porous media [11, 12], or the liquid transport which can be described by Darcy's law [7, 13–15], or as capillary tubes, where the liquid flow can be modelled by Lucas–Washburn kinetics [16–18]. In the first case, however, the characteristic parameters, such as permeability, are difficult to quantify and are always obtained empirically [14, 15, 19]. In the second case, similarly, the effective radius of the capillary tube, the effective contact angle, etc., are also determined by fitting the experimental data [20].

Different fabric structures were investigated to improve fabric-wearing comfort. Water permeability is one of the important parameters to be considered when designing functional fabrics [21–24].
Based on the Forchheimer law a forced water permeability was determined using a developed experimental setting on the textile fabric in the plane direction [25]. This method could be used for technical textile applications for water filters or tranquilizers. The pressure gradient range was from 1000 to 4000 Pa within a water velocity range of 0 to 5 cm/s. These values are tremendous and outside the range of liquid diffusion during a wicking test where the highest water velocity was about $2 \cdot 10^{-2}$ cm/s for larger pores equivalent radius of about $16.6 \cdot 10^{-4}$ m [26]. A literature review previously mentioned by [9–12, 19, 20, 27, 28], shows that although broad research has been carried out in this area, a procedure to determine the in-plane water permeability during wicking through textile-based is still lacking.
In this work, in-plane water permeability during combined wicking (ascendant, horizontal and descendant) was determined. Based on the assumptions that a liquid front flow and the saturation rate are constant, a mathematical model was developed using the second Archie's law and the Luca-Washburn equation. An experimental validation showed that our model can correctly determine the spatiotemporal distribution of saturation rate in textile structure.

WATER PERMEABILITY MATHEMATICAL FORMULATION

The single-phase flow of a Newtonian liquid in an isotropic and rigid porous medium is governed by Darcy's law [29]:

$$V = -\frac{K}{\mu}(\text{grad}\, P - \rho g) \tag{1}$$

It could be written as follows:

$$V = -\frac{K}{\mu}\left(\frac{dP}{dh}\right) \tag{2}$$

where V is Darcy velocity, also called specific discharge vector (m/s), K – liquid permeability [m^2], μ – liquid dynamic viscosity (Pa·s), P – liquid pressure in the pores (Pa), ρ – liquid density (Kg/m^3), g – gravitational acceleration (m/s^2), h – liquid front position (m).
Based on the hypothesis of constant fluid flow speed and a constant saturation rate, two hypotheses should be considered when evaluated to evaluate the water permeability during a combined wicking test:
- the fluid flow is constant,
- the saturation rate is constant.

The continuity equation is:

$$\frac{dV}{dh} = 0 \tag{3}$$

Combining equations 2 and 3, the pressure distribution in the wetted area is governed by the following equation:

$$\frac{d^2P}{d^2h} = 0 \tag{4}$$

Here (μ) is constant and also (K) for a given saturation rate (S), the integration of the equation 4 will be as follows:

$$P(h) = Ah + B \tag{5}$$

where A and B are constant. The boundary conditions for equation 5 can be deduced as:

$$P = P_{atm} \text{ at } h = 0 \tag{6a}$$

$$P = P_{atm} - (P_C - S\rho g h_f) \text{ at } h = h_f \tag{6b}$$

where P_{atm} is atmospheric pressure (Pa), P_C – capillary pressure (Pa), h_f – liquid front height (m), S – saturation rate.
So, $P = B = P_{atm}$ and $P(h_f) = Ah_f + P_{atm} = P_{atm} + S\rho g h_f - P_C$. Consequently $A = S\rho g - \frac{P_C}{h_f}$. This leads to the pressure in the wetted zone:

$$P(h) = P_{atm} + S\rho g h - \frac{h}{h_f} P_C \text{ for } 0 \le h \le h_f \tag{7}$$

The liquid front speed for a given liquid height (h_f) based on the Darcy front speed as mentioned in equation 2, is:

$$\frac{dh_f}{dt} = \frac{V(h=h_f)}{\varepsilon} = -\frac{K}{\varepsilon\mu}\frac{dP}{dh} \tag{8}$$

Here the porosity (ε) was added to the equation to calculate the macroscopic liquid front speed from the liquid speed in the pores. Using equation 7, the macroscopic liquid front speed is:

$$\frac{dh_f}{dt} = -\frac{K}{\varepsilon\mu}\left(\frac{P_C}{h_f} - S\rho g\right) \tag{9}$$

The rearrangement of the Equation 9 leads to:

$$\frac{\varepsilon\mu}{K} h_f \frac{dh_f}{dt} = P_C - S\rho g h_f \tag{10}$$

Supposedly,

$$G = P_C - S\rho g h_f \tag{11}$$

So, $h_f = \frac{P_C - G}{S\rho g}$; $\frac{dh_f}{dt} = -\frac{1}{S\rho g}\frac{dG}{dt}$, at $h_f(0) = 0$ and $G(0) = P_C$. Replacing (G) in the equation 10 leads to:

$$\frac{\varepsilon\mu}{K}\left(\frac{P_C - G}{S\rho g}\right)\left(-\frac{1}{S\rho g}\frac{dG}{dt}\right) = G \tag{12}$$

Using the variable separation method, the resulting equation is:

$$\frac{\varepsilon\mu}{KS^2\rho^2 g^2}\left(dG - P_C\frac{dG}{G}\right) = dt \tag{13}$$

The integration of the equation 13 leads to:

$$\frac{KS^2\rho^2 g^2}{\varepsilon\mu} t = G + C_1 - P_C \ln(G) + C_2 \tag{14}$$

where (C_1) and (C_2) are constants to be determined based on the following boundary conditions:
$G(0) = P_C$ at $t = 0$. So $P_C + C_1 - P_C \ln(P_C) + C_2 = 0$.
So, Equation 14 becomes:

$$\frac{KS^2\rho^2g^2}{\varepsilon\mu}t = G - P_C\ln(G) + P_C\ln(P_C) - P_C \quad (15)$$

Replacing (G) by it expression in the equation 11 in the Equation 15, leads to:

$$P_C\ln\left(\frac{P_C}{P_C - S\rho g h_f}\right)S\rho g h_f = \frac{KS^2\rho^2g^2}{\varepsilon\mu}t \quad (16)$$

Based on this combined wicking configuration (ascendant, horizontal and descendant), to determine the permeability as a function of the saturation rate, equation 17 of the hydrostatic pressure (P_h) was considered considering the saturation rate (S) at the liquid front position (h_f):

$$P_{h_f} = S\rho g h_f \quad (17)$$

To evaluate the permeability using this method, the following equation deduced from equation 9 is introduced:

$$K = \frac{\frac{dh_f}{dt}h_a\mu}{(P_C + P_{h_f})} \quad (18)$$

Here, the capillary pressure at each saturation rate should be known and it is expressed as follows:

$$P_C = \frac{2\gamma_L\cos\theta}{R_C} \quad (19)$$

When the effective capillary radius (R_C) as a function of the saturation rate is known, equation 18 is used to calculate the liquid permeability value at a height (h_f) and a saturation rate (S). In fact, by changing the ascendant wicking height (h_a), permeability values could be generated at each saturation rate.

The effective capillary radius (R_C) is determined using a horizontal wicking test. In fact, for most porous materials, subjected to a horizontal impregnation test, the gravitational force can be neglected [30]. Some researchers [9, 10, 31–33] have proposed that the liquid front position (h_f) can be expressed by the Washburn equation:

$$h_f^2 = \frac{\gamma_L R_C\cos\theta}{2\mu}t \quad (19)$$

According to equation 20, the curve $h_h = f(\sqrt{t})$ has a linear form if the following conditions and assumptions are verified:

- the physical properties of the liquid are constant throughout the system,
- the average equivalent capillary radius is constant,
- the system is supplied with liquid from an infinite reservoir.

The slope (C_D) of the curve $h_h = f(\sqrt{t})$, called wetting coefficient [27] or diffusion rate, is given by the following equation:

$$Slope = C_D = \sqrt{\frac{\gamma_L R_C\cos\theta}{2\mu}} \quad (21)$$

Thus, the diffusion coefficient (C_D) is used to determine the effective capillary radius (R_C) as follows:

$$R_C = C_D^2\left(\frac{2\mu}{\gamma_L\cos\theta}\right) \quad (22)$$

In the combined wicking test (ascendant, horizontal and descendant), by changing the ascendant position during ascendant wicking, it is possible to determine the diffusion coefficients (C_D) and capillary radii (R_C) at different saturation rates (S). The last mentioned found values can be used for the calculation of the capillary pressure (P_C). Using the latter, we can determine the permeability using equation 18.

MATERIALS AND METHODS

Used materials

Combined wicking tests were conducted on four plain knitted fabrics and using a cotton yarn with 88 fibres per section have an average diameter of about 15 μm. The yarn count was 15 Nm with an average diameter of $7.44\cdot10^{-4}$ m. A Stoll CMS 320 TC C - 530 010 Flat knitting machine gauge 7 was used to knit used samples. The distilled water with a density of 998.29 kg/m^3, a Dynamic viscosity of 0.001003 Kg/m·s and a Contact angle/cotton fibre $\cos\theta$ = 0.97 was used as a wetting liquid

The fabric thickness (T_h) was determined according to the NF G 07-153 standard using Digital Thickness Gauge from SDL Atlas. The loop length (L_{loop}), the number of wales (W) and courses (C) per centimetre were measured according to the standard NF G 07-101 using the Crimp-Tester from Sodemat.

Wicking through the textile fabrics can be regarded as a liquid transfer through a porous media structure with tortuous channels and via macro and micropore scales. So, The liquid wicking through a textile knitted fabrics is defined as tortuous capillary tubes in the scale of the yarns (porosity scale between fibres) and a distance plates (porosity scale between yarns) [26]. The tortuosity (τ), is defined as below [26]:

$$\tau = \frac{L_{loop}C}{2} \quad (23)$$

Here (L_{loop}) is the loop length in cm and (C) is the course density per cm.

The mean micro pores radius (R_{mi}) (porosity between fibers) is determined as follows [20, 26]:

$$R_{mi} = \sqrt{\frac{t_h^2}{32n_s} - \frac{t_{fiber}^2}{8}} \quad (24)$$

The capillary rise between yarns (on the fabric scale) can be regarded as equivalent to a flow between two distant parallel plates [20, 26]. The equivalent distance (e_{mac}) is:

$$e_{mac} = \frac{1}{W} - \frac{\pi C d_{yarn}^2}{2t_h}L_{loop} \quad (25)$$

The structural properties of the used jersey knitting are shown in table 1.

All wicking tests were carried out in a standard atmosphere of 20±2°C as test temperature and 65±2%

Table 1

THE CHARACTERISTICS OF THE USED KNITTED FABRICS				
Sample	**1**	**2**	**3**	**4**
Loop length (cm)	0.51 ± 0.02	1.10 ± 0.03	0.93 ± 0.02	0.74 ± 0.01
Wales/cm	5.0 ± 0.2	3.4 ± 0.1	3.8 ± 0.2	2.8 ± 0.1
Courses/cm	6.0 ± 0.3	4.8 ± 0.2	5.8 ± 0.2	3.0 ± 0.1
t_h (mm)	2.01 ± 0.02	2.06 ± 0.03	1.89 ± 0.01	1.01 ± 0.02
Tortuosity (τ)	1.53 ± 0.04	2.65 ± 0.03	2.69 ± 0.02	1.11 ± 0.01
e_{mac} (10^{-4} m)	6.7 ± 0.3	7.01 ± 0.02	1.58 ± 0.01	16.66 ± 0.05
R_{mi} (10^{-5} m)	3.73 ± 0.05	3.84 ± 0.06	3.53 ± 0.04	1.82 ± 0.03

Note: n_s – number of fibres per cross section; t_h – fabric thickness; Courses/cm – courses density; Wales/cm – wales density; Nm – metric numbering system (number of 1 km of yarn per 1 kg weight); e_{mac} – equivalent distance between two plates (case of wicking in the macro pores scale); R_{mi} – average capillary radius (case of wicking in the micro pores scale).

of relative humidity. Samples were conditioned for 24 hours before testing.

Ascendant-horizontal-descendant wicking configuration

Combined wicking experimental setup

The experimental configuration of the ascendant-horizontal-descendant wicking from an infinite reservoir was used as illustrated in figure 1. This combined wicking configuration allows us to follow the saturation rate using an electrical resistivity meter and the liquid flow speed for each wicking type using a CCD camera.

To slowly raise the reservoir containing the wicking liquid to avoid the first contact with the fabric/liquid at the first stage of wicking a laboratory jack was used. The effect of liquid evaporation from the liquid reservoir was reduced by employing an attached gap plate and allowing sample permeation and wicking [34].

Liquid front speed measurement

The liquid front speed for different wicking configurations (Ascendant, horizontal and downward) was observed and measured using a CCD camera by periodically taking snapshots. The corresponding time and wicking front were continuously recorded until equilibrium was established. In the first stage, all images were processed to adjust brightness, size cropping, and image calibration using Photoshop software. In the second stage, the liquid front was obtained using a developed Matlab program. Where all captured images were first converted to a grey level, the contrast of a grayscale image was then adjusted using histogram equalization. In the image, dark areas refer to wetted regions and clear ones to non-wetted fabric regions. To calculate the liquid front, all binarized image pixels were examined.

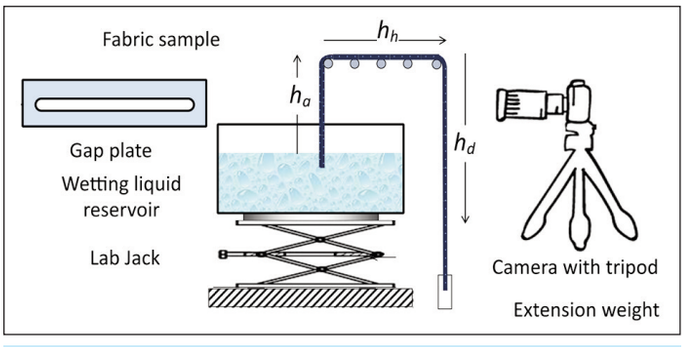

Fig. 1. Experimental configuration of the ascendant (h_a), horizontal (h_h) and descendant (h_d) wicking test from an infinite reservoir

Saturation rate determination

The saturation rate (S) was determined using the electrical resistivity method. The 4339B high-resistance meter from Agilent® was used to measure the electrical resistivity.

The second Archie's law defines the saturation related to the resistivity index (I_R), as expressed by the following equation [35]:

$$I_R = \frac{R_{e-m}}{R_{e-sat}} = \frac{1}{S^n} \quad (26)$$

Here R_{e-m} (Ω·m) is the bulk effective resistivity of the porous material, R_{e-sat} (Ω·m) is the saturated porous media resistivity and (n) the exponent of "Archie saturation" which is close to 2 but can reach 10 [13].

A calibration process was carried out for all samples for different saturation rates using the electrical resistivity method. Firstly, a dried sample with dried mass m_d (g) was immersed in a wetting liquid. Then, the mass of the wetted sample m_w (g) is continuously recorded by an electrical balance to determine the saturation rate (S) using the following equation:

$$S = \frac{m_w - m_d}{m_d} \quad (27)$$

As illustrated in the sample 1 calibration for the saturation exponent (n) determination (figure 2). It is noticed that the regression line of the curve $\ln\left(\frac{R_{e-m}}{R_{e-sat}}\right) = f(\ln(S))$ is linear with a coefficient of determination $R^2 = 0.9921$ and $n = 2.6104$ with a standard deviation of 0.0152 and a CV of 1.614%.

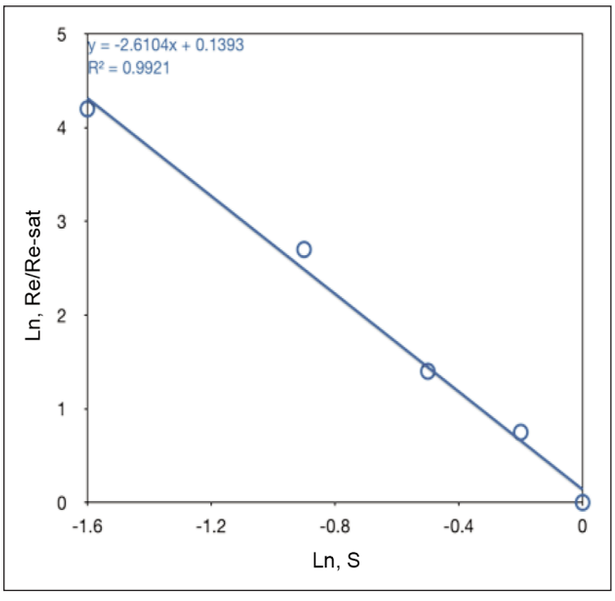

Fig. 2. Saturation exponent (n) determination using electrical resistivity calibration for sample 1

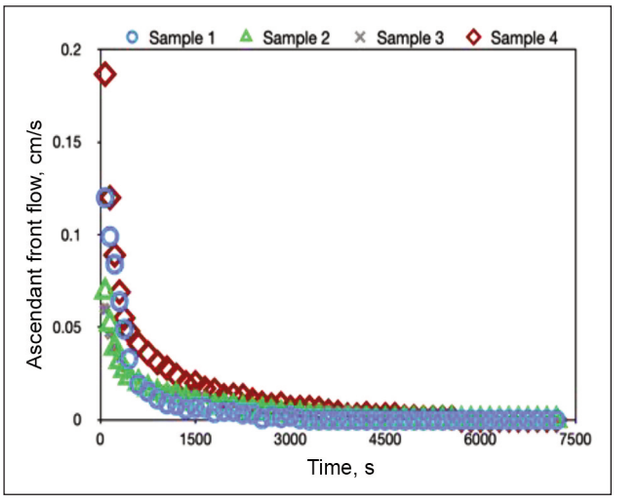

Fig. 3. Tested fabrics experimental ascendant liquid front flow

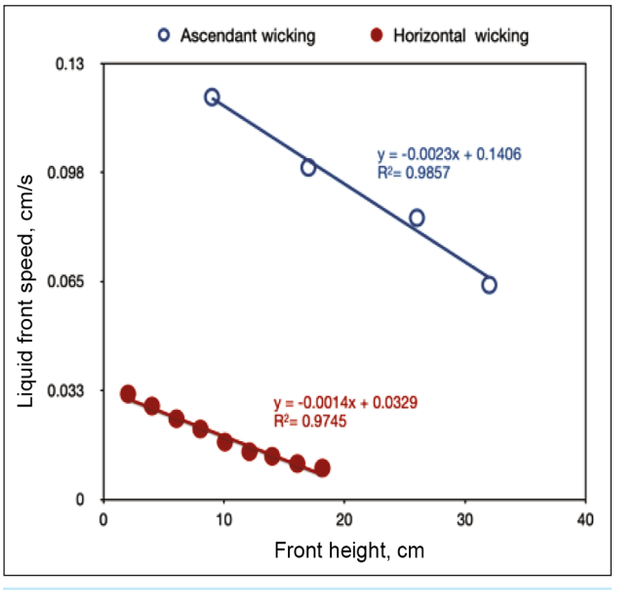

Fig. 4. Liquid front speed as a function of front position during ascendant and horizontal wicking case sample (1)

In the case of sample 2, the calibration results were a coefficient of determination $R^2 = 0.9692$ and $n = 4.4652$ with a standard deviation of 0.0236 and a CV of 1.782%. For the sample 3 results were a coefficient of determination $R^2 = 0.9553$ and $n = 3.6952$ with a standard deviation of 0.0146 and a CV of 1.411%. In the case of sample 4, the most permeable one, calibration results were, a coefficient of determination $R^2 = 0.9835$ and $n = 3.0264$ with a standard deviation of 0.0133 and a CV of 1.667%.

RESULTS AND DISCUSSION

As mentioned in the previous section, two hypotheses should be considered when evaluating the water permeability during a combined wicking test: fluid flow and saturation rate are constant. So, preliminary tests were conducted to verify the two assumptions.

Liquid front speed during ascendant, horizontal and descendant wicking

Figure 3 illustrates the experimental results of the front velocity for the ascendant wicking test for the studied samples. It is noticed that the liquid front speed decreases as a function of time. At short times, this speed is significant and then decreases to reach zero speed at the equilibrium.

Indeed, the speed is important at the beginning because it involves the filling of the macro-channels which serve as reservoirs for the filling of the micro-channels.

The sample (4) having the largest macro-pore size ($e_{mac} = 16.6 \cdot 10^{-4}$ m) has an initial ascent speed of around 0.186 cm/s which is the highest compared to the other samples.

By comparing the two cases ascendant and horizontal wicking, it is clear the front speed deceleration during the ascendant wicking test is about 0.0023 m/s^2 and more significant compared to the horizontal one which is about 0.0014 m/s^2 as illustrated in figure 4. Gravitational forces act in the opposite direction to capillary rise.

In this part, the liquid front speed in a combined horizontal-descending wicking test was experimentally studied as configurated in the experimental set-up (figure 1). This test was carried out according to the principle of horizontal followed by descending wicking. The liquid front speed during this combined test is presented in figure 5.

The combined wicking test (horizontal and descendant) was carried out at an ascendant wicking height position (h_a) of 4 cm. It was observed that liquid front speed during the horizontal wicking is decreasing with an initial speed equal to 0.0314 cm/s with a standard deviation of 0.0015 and a CV of 1.216%. During the descendant wicking, the liquid front speed is constant at about 0.006469 cm/s with a standard deviation of 0.000816 and a CV of 2.079%.

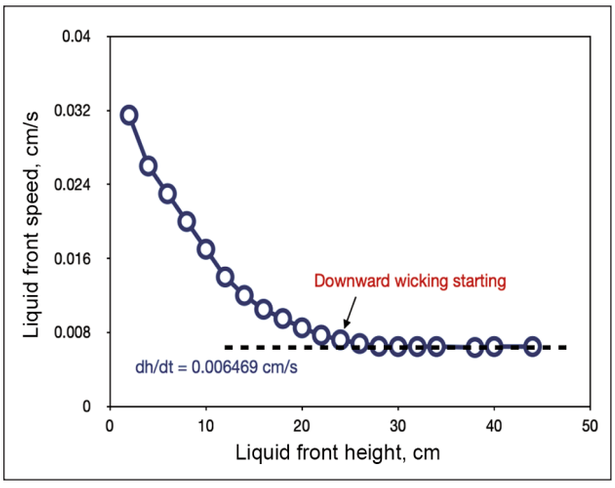

Fig. 5. Liquid front speed as a function of front position during combined horizontal and descendant wicking case sample (1)

In the case of the ascendant wicking test, the viscous forces opposed to the capillary forces, the effect of gravity should be added, which exerts a force in the opposite direction to the direction of the ascendant liquid front. An equilibrium state, corresponding to zero liquid speed, results in this case in equality between the capillary forces and the sum of the gravitational and viscous forces. Whereas in the case of horizontal wicking, the effect of the gravitational force is zero given that the direction of movement of the liquid is perpendicular to gravity. Thus, it is only the viscosity forces that attenuate the advancement of the front.

It could be concluded that the liquid front is decreasing in the case of ascendant and horizontal wicking tests, while it is constant in the case of descendant wicking.

Saturation rate during ascendant, horizontal and descendant wicking

Figure 6 illustrates the spatiotemporal distribution of saturation rate in the case of an ascendant wicking test at 4 cm steps. At the same liquid front position, the saturation rate is identical which implies the structure properties are the same along the width. Not surprisingly, the liquid saturation rate in an early stage is much higher than in subsequent stages. With time passing, the liquid rise speed becomes slower, caused by the gravitational forces slowing down the liquid ascendant flow, until equilibrium is established. Figure 7 presents the variation in saturation rate in the case of horizontal and descending wicking at different vertical positions (h_a) at 4 cm and 8 cm.

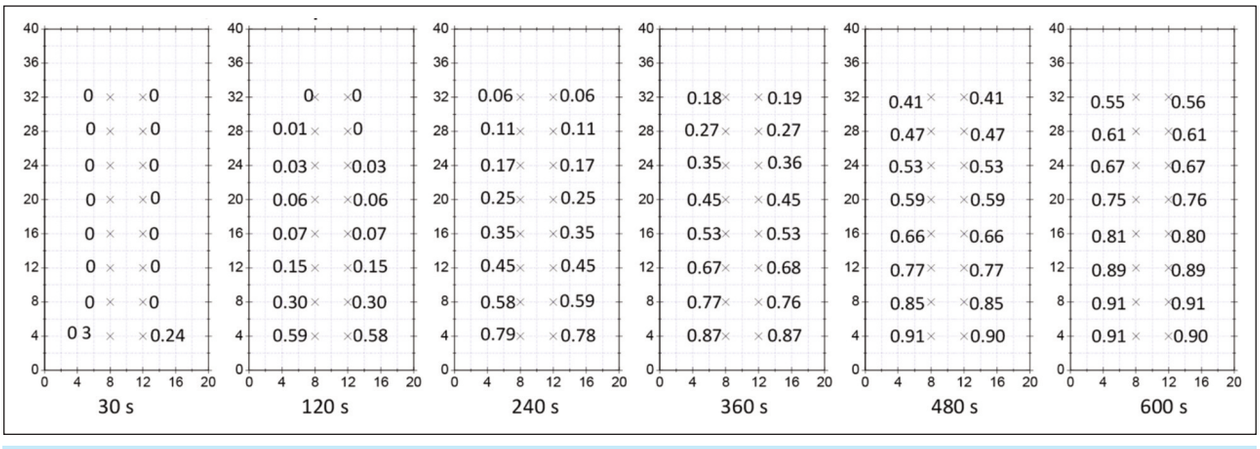

Fig. 6. Saturation rate spatiotemporal distribution during ascendant wicking test

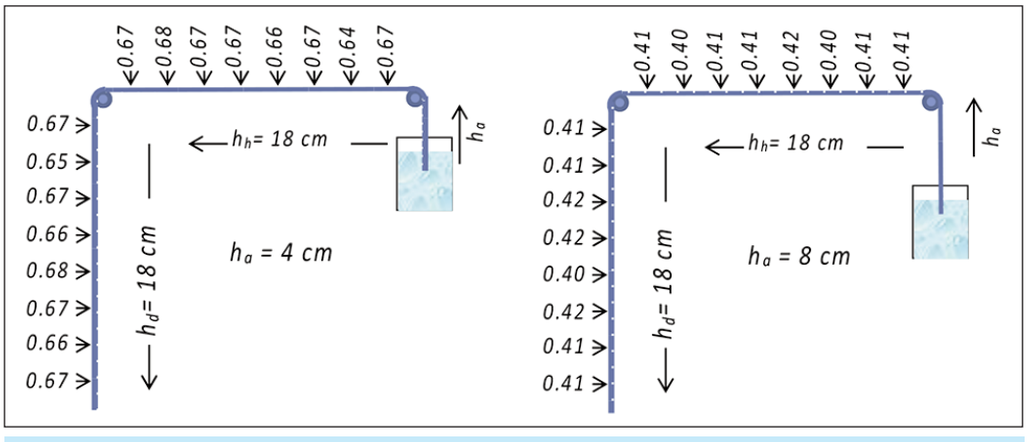

Fig. 7. Saturation rate during horizontal (h_h) and descendant (h_d) wicking test at 2 cm intervals from the infinite reservoir

According to figure 7, It is noticed that in the case of h_a = 4 cm, the average saturation rate is about 0.6675 (standard deviation of 0.0093 and a CV of 1.394%). Whereas for h_a = 8 cm, the average saturation rate is about 0.4106 (standard deviation of 0.0068 and a CV of 1.65%).

So, it can be concluded that the saturation rate is constant during the horizontal and descending wicking. Moreover, the average saturation rate is inversely proportional to the vertical position from the reservoir. Indeed, by increasing (h_a), the saturation rate becomes smaller at the horizontal and descending wicking level caused by the effect of gravitational forces.

Based on the preliminary combined wicking tests the following founds could be affirmed:

- During the ascendant wicking: the liquid front speed and the saturation rate are not constant and decline with the liquid front position.
- During the horizontal wicking: the liquid front speed is not constant and declines with the liquid front position. On the contrary, the saturation rate is constant for any liquid front position.
- During the descendant wicking: liquid front speed and saturation rate are constant for any liquid front position.

The three combined wicking tests (ascending, horizontal and descending) were used to determine the two fundamental properties of textile materials to characterize wetting behaviour: capillary pressure and permeability at different saturation rates.

The ascendant height was varied during the ascendant wicking test to adjust the saturation rate during the horizontal and the descendant wicking tests. A horizontal wetting test was used to calculate the effective capillary radius of the textile fabric by exploiting equation 22, which will be used to calculate the capillary pressure through equation 19. The last-mentioned property was used to calculate the liquid permeability during the descendant wicking based on equation 18.

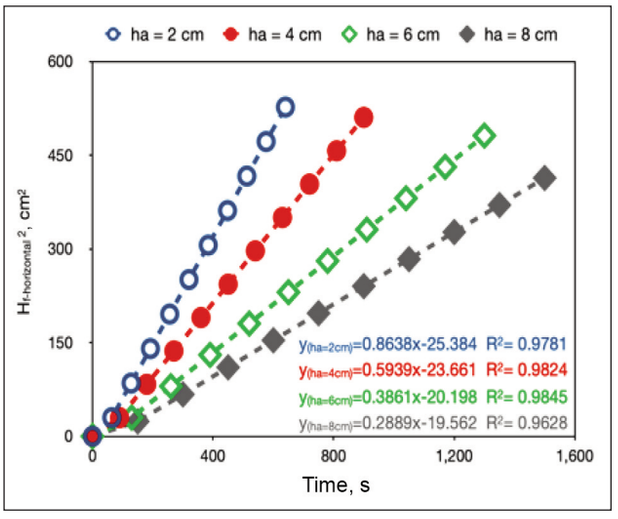

Fig. 8. Squared liquid front height during the horizontal wicking test for different vertical position ascendant wicking (h_a) test: case sample (1)

Wicking parameters

By Plotting the curve of the squared liquid front as a function of time during the horizontal wicking test, it is possible to calculate the diffusion coefficient. presents the squared liquid front height during the horizontal wicking test for different vertical position ascendant wicking (h_a) tests in the case of the sample (1).

According to figure 8, it is noted that the shape of the curves follows a linear form with a regression coefficient (R^2) varying from 0.96 to 0.98. In addition, the slope decreases with the liquid vertical position (h_a). Indeed, at h_a = 2 cm, the slope is about 0.8638 cm^2/s with a standard deviation of 0.0293 and a CV of 1.512%, while at the ascendant vertical position of h_a = 8 cm, the slope is about 0.2889 cm^2/s with a standard deviation of 0.0186 and a CV of 1.956%. This is explained by the greater the vertical position (h_a) becomes, the more the front moves less quickly and the saturation decreases.

Table 2

SATURATION RATE (S) AND DIFFUSION COEFFICIENT (C_D) DURING HORIZONTAL WICKING TESTS AT DIFFERENT ASCENDANT HEIGHTS (h_a)

Vertical position ascendant wicking (h_a) (cm)	Level	Parameters	Fabric sample (1)	(2)	(3)	(4)
	2	S	0.718 ± 0.002	0.923 ± 0.004	0.883 ± 0.003	0.771 ± 0.002
		C_D (cm/s$^{1/2}$)	0.929 ± 0.011	1.207 ± 0.010	0.787±0.009	1.123 ± 0.008
	4	S	0.667 ± 0.008	0.841 ± 0.005	0.779 ± 0.003	0.659 ± 0.001
		C_D (cm/s$^{1/2}$)	0.771 ± 0.010	1.088 ± 0.008	0.648 ± 0.007	1.003 ± 0.008
	6	S	0.531 ± 0.005	0.735 ± 0.006	0.685 ± 0.005	0.576 ± 0.002
		C_D (cm/s$^{1/2}$)	0.621 ± 0.006	0.904 ± 0.007	0.502 ± 0.000	0.929 ± 0.012
	8	S	0.412 ± 0.004	0.657 ± 0.005	0.562 ± 0.006	0.493 ± 0.002
		C_D (cm/s$^{1/2}$)	0.537 ± 0.009	0.784 ± 0.008	0.427 ± 0.005	0.675 ± 0.007

Assuming that the Lucas-Washburn equation remains valid in our case, the effective capillary radius (R_C) of each sample is determined by knowing the diffusion coefficient (C_D) in the horizontal impregnation test and using equation 22.

Once known, at each height (h_a), the effective capillary radius (R_C) is used to calculate the capillary pressure (P_C) using equation 19. This last physical property (PC) is used, at different saturation rates, for the calculation of permeability using equation 18.

To calculate the permeability using equation (18), and at different saturation rates, we must know the descent liquid front speed $\left(\frac{dh_f}{dt}\right)$. The descent liquid flow was varied with the ascendant liquid position (h_a) from 2 to 8 cm.

Figure 9 illustrates the squared height during a descendant wicking test preceded by ascendant and horizontal wicking. The horizontal wicking test was carried out over a length of 18 cm followed by a descent wicking test over a length of 18 cm. The position of the front as a function of time is linear regardless of the ascendant liquid position. In addition, this speed decreases with ascendant height position (h_a). The linear regression coefficient (R^2) ranges from 0.96 to 0.99.

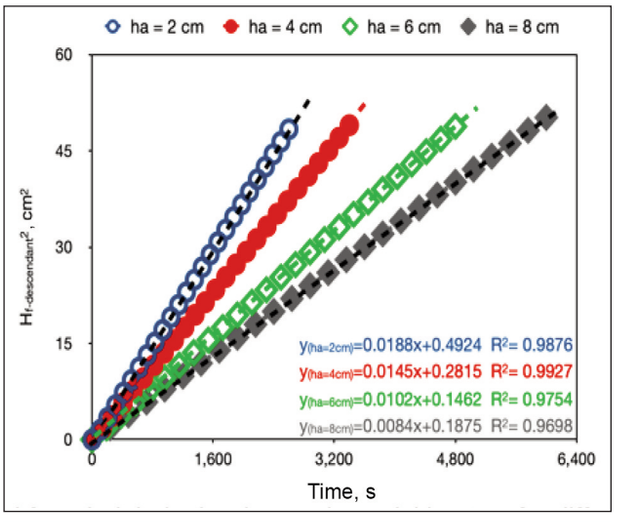

Fig. 9. Squared liquid front height in the descendant wicking test for different vertical position ascendant wicking (h_a) test: case sample (1)

Thus, the fundamental wicking parameters are obtained for different vertical ascendant positions (h_a): Saturation rate (S), effective average capillary radius (R_C), capillary pressure (P_C), water-front speed and in-plane water permeability (K), as presented in table 3.

Table 3

WICKING PARAMETERS DURING DESCENDANT WICKING AT DIFFERENT VERTICAL POSITION ASCENDANT WICKING (h_a): SATURATION RATE (S), EFFECTIVE AVERAGE CAPILLARY RADIUS (R_C), CAPILLARY PRESSURE (P_C), WATER-FRONT SPEED AND IN-PLANE WATER PERMEABILITY (K)

Vertical position ascendant wicking (h_a) (cm)	Level	Wicking parameters	Fabric sample			
			(1)	(2)	(3)	(4)
	2	S	0.718 ± 0.002	0.923 ± 0.004	0.883 ± 0.003	0.771 ± 0.002
		R_C (μm)	2.464 ± 0.015	4.154 ± 0.022	1.767 ± 0.009	3.597 ± 0.018
		P_C (10^5 dynes/cm^2)	5.708 ± 0.029	3.386 ± 0.017	7.962 ± 0.039	3.910 ± 0.019
		Liquid front speed (cm/s)	0.0188 ± 0.0095	0.0152 ± 0.0076	0.0129 ± 0.0064	0.0246 ± 0.0023
		K (10^{-10} cm^2)	6.371 ± 0.031	8.337 ± 0.041	3.148 ± 0.015	11.932 ± 0.005
	4	S	0.667 ± 0.008	0.841 ± 0.005	0.779 ± 0.003	0.659 ± 0.001
		R_C (μm)	1.694 ± 0.009	3.378 ± 0.017	1.199 ± 0.006	2.868 ± 0.015
		P_C (10^5 dynes/cm^2]	8.302 ± 0.041	4.163 ± 0.021	1.173 ± 0.005	4.903 ± 0.025
		Liquid front speed (cm/s)	0.0145 ± 0.0074	0.0123 ± 0.0062	0.0107 ± 0.0051	0.0202 ± 0.0012
		K (10^{-10}cm^2)	3.423 ± 0.017	5.594 ± 0.028	1.795 ± 0.011	8.777 ± 0.044
	6	S	0.531 ± 0.005	0.735 ± 0.006	0.685 ± 0.005	0.576 ± 0.002
		R_C (μm)	1.101 ± 0.005	2.331 ± 0.011	0.718 ± 0.003	2.463 ± 0.012
		P_C (10^5 dynes/cm^2)	1.277 ± 0.005	6.035 ± 0.030	1.958 ± 0.021	5.710 ± 0.028
		Liquid front speed (cm/s)	0.0102 ± 0.0056	0.0109 ± 0.0061	0.0082 ± 0.0041	0.0202 ± 0.0016
		K (10^{-10}cm^2)	1.583 ± 0.009	3.498 ± 0.018	0.831 ± 0.005	6.893 ± 0.038
	8	S	0.412 ± 0.004	0.657 ± 0.005	0.562 ± 0.006	0.493 ± 0.002
		R_C (μm)	0.824 ± 0.004	1.755 ± 0.009	0.520 ± 0.002	1.301 ± 0.006
		P_C (10^5 dynes/cm^2)	1.707±0.008	8.015 ± 0.005	2.705±0.001	1.081 ± 0.002
		Liquid front speed (cm/s)	0.0084 ± 0.0048	0.0081 ± 0.0043	0.0069 ± 0.0039	0.0193 ± 0.0009
		K (10^{-10}cm^2)	0.980 ± 0.006	1.980 ± 0.012	0.508 ± 0.002	4.582 ± 0.088

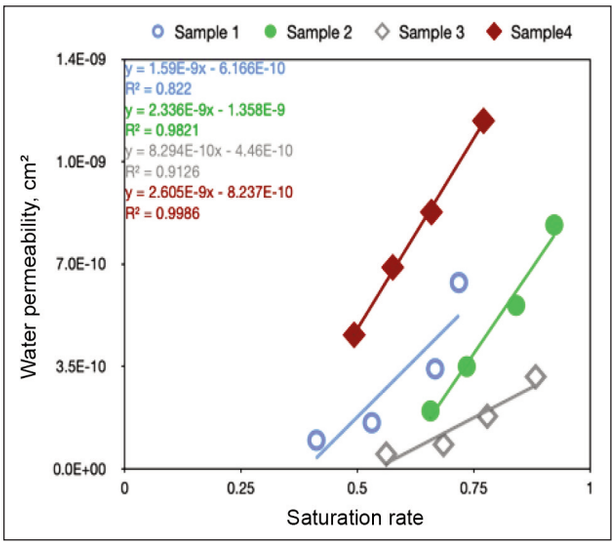

Fig. 10. Effect of saturation rate on in-plane water permeability

The evolution of permeability as a function of the saturation rate is illustrated in figure 10. It is pointed out that the permeability is variable and depends on the saturation rate. In addition, sample (4) is the most permeable of all the samples regardless of the saturation rate. Indeed, the size of the macro-pores is of the order of $16.6 \cdot 10^{-4}$ m which is the largest compared to the other samples.

According to figure 10, there is a linear relationship between water permeability and saturation rate. For example, in the sample (4), the regression coefficient is about $2.605 \cdot 10^{-9}$ with an R^2 of 0.9986. In the case of sample (3), the regression coefficient is about $8.298 \cdot 10^{-9}$ with R^2 of 0.9126 which is less permeable with smaller pores size of about $1.58 \pm 0.01 \cdot 10^{-4}$ m compared to sample (4) with macro-pores sized of about $16.66 \pm 0.05 \cdot 10^{-4}$ m. Thus, with higher pore size and saturation rate, the prewetting liquid film improves the liquid spreading in the pores scale and subsequently makes the fabric more permeable to the water.

CONCLUSIONS

The in-plane water permeability was investigated in this paper during wicking. Based on the two assumptions (the saturation rate and liquid front speed are constant) a mathematical formulation of the in-plane liquid permeability during combined wicking (ascendant, horizontal and descendant) was introduced by exploiting the Darcy law and le Luca-Washburn equation.

An experimental setup was designed to experimentally follow the combined wicking and to measure the water in-plane permeability for different saturation rates. The saturation rate was determined using an electrical resistivity meter based on the second Archie law and the liquid flow speed was measured for the three wicking configuration tests using a CCD camera at different liquid front positions. Preliminary tests were carried out to verify the two mentioned assumptions.

The study of the liquid front speed of three wicking types showed that, in the case of an ascendant and a horizontal wicking test, the liquid front speed decreases and the liquid front speed deceleration is more significant during the ascendant wicking compared to the horizontal one. Whereas in the case of a descendant wicking, this speed remains constant.

Based on the electrical method and using Archie's second law, the saturation spatiotemporal distribution of saturation was determined for different wicking tests. It was found that in the case of ascendant wicking, the saturation rate decreases with the liquid front height position. Whereas in the horizontal and descendant wicking, the saturation is uniform and remains constant regardless of the horizontal position height (h_a). By varying the vertical height of the horizontal part relative to the reservoir, the saturation rate decreases.

Capillary pressure and permeability at different saturation rates were determined. A variation in the vertical position of the sample relative to the reservoir (h_a) allows us to adjust the saturation rate during wicking. For the descendant wicking, where the liquid flow and the saturation rate are constant, the in-plane water permeability was calculated. The water in-plane permeability is linearly related to the saturation rate. Tested fabrics with larger macro pores are more porous. The formed liquid film in the pore scales enhances the liquid spreading and so makes the fabric more permeable to water.

Nevertheless, this research attempts to gain insight into this area and to construct a framework for further studies. Improving the fabric in-plane water permeability during wicking will form the subject of subsequent research.

REFERENCES

[1] Yoo, S., Barker, R.L., *Moisture Management Properties of Heat-Resistant Workwear Fabrics – Effects of Hydrophilic Finishes and Hygroscopic Fiber Blends*, In: Text. Res. J., 2004, 74, 995–1000, https://doi.org/10.1177/004051750407401110

[2] Soltani, M., Lahiri, S.K., Shabanian, S., Golovin, K., *Surface-engineered double-layered fabrics for continuous, passive fluid transport*, In: Mater. Horizons, 2023, 10, 4293–4302, https://doi.org/10.1039/d3mh00634d

[3] Abada, D., Maalouf, C., Sotehi, O., Rouag-Saffidine, D., Polidori, G., Boudjabi, A.F., et al., *Performance evaluation of fabrics for evaporative cooling applications*, In: Energy Build., 2022, 266, https://doi.org/10.1016/j.enbuild.2022.112120

[4] Matusiak, M., Kamińska, D., *Liquid Moisture Transport in Cotton Woven Fabrics with Different Weft Yarns*, In: Materials (Basel), 2022, 15, https://doi.org/10.3390/ma15186489
[5] Peng, Y., Li, W., Liu, B., Jin, W., Schaadt, J., Tang, J., et al., *Integrated cooling (i-Cool) textile of heat conduction and sweat transportation for personal perspiration management*, In: Nat. Commun., 2021, 12, https://doi.org/10.1038/s41467-021-26384-8
[6] Lei, M., Li, Y., Liu, Y., Ma, Y., Cheng, L., Hu, Y., *Effect of weaving structures on the water wicking-Evaporating behavior of woven fabrics*, In: Polymers (Basel), 2020, 12, https://doi.org/10.3390/polym12020422
[7] Suresh, S.S., Raja, D., Thiyaneswaran, B., Gobinath, R., Kumar, S.K.S., Panneerselvam, R.G., et al., *A novel conductive sensor-based test method to measure longitudinal wicking of fabrics*, In: Indian J. Fibre Text. Res., 2022, 47, https://doi.org/10.56042/ijftr.v1i2.54667
[8] Adamu, B.F., Gao, J., *Comfort related woven fabric transmission properties made of cotton and nylon*, In: Fash. Text., 2022, 9, https://doi.org/10.1186/s40691-021-00285-2
[9] Hollies, N.R.S., Kaessinger, M.M., Bogaty, H., *Water Transport Mechanisms in Textile Materials1 Part I: The Role of Yarn Roughness in Capillary-Type Penetration*, In: Text. Res. J., 1956, 26, 829–835, https://doi.org/10.1177/004051755602601102
[10] Hollies, N.R.S., Kaessinger, M.M., Watson, B.S., Bogaty, H., *Water Transport Mechanisms in Textile Materials Part II: Capillary-Type Penetration in Yarns and Fabrics*, In: Text. Res. J., 1957, 27, 8–13, https://doi.org/10.1177/004051755702700102
[11] Amico, S.C., Lekakou, C., *Axial impregnation of a fiber bundle. Part 1: Capillary experiments*, In: Polym. Compos., 2002, 23, 249–263, https://doi.org/10.1002/pc.10429
[12] Amico, S.C., Lekakou, C., *Axial impregnation of a fiber bundle. Part 2: Theoretical analysis*, In: Polym. Compos., 2002, 23, 264–273, https://doi.org/10.1002/pc.10430
[13] Toumelin, E., *Pore-scal petrophysical models for the simulation and combined interpretation of nuclear magnetic resonance and wide-band electromagnetic measurements of saturated rocks*, The University Of Texas at Austin, 2006
[14] Adámek, K., Havelka, A., Kůs, Z., Mazari, A., *The Correlation between Air and Water Vapour Permeability of Textiles*, In: Coatings, 2023, 13, https://doi.org/10.3390/coatings13010163
[15] Mazari, A., Havelka, A., Naeem, J., Adamek, K., *Comparative study on the water vapour permeability of textile by a standard and novel device*, In: Fibres Text. East. Eur., 2021, 29, https://doi.org/10.5604/01.3001.0015.2724
[16] Subramaniam, V., Raichurkar, P., *A review on wicking of yarns and fabrics*, In: Int. J. Text. Eng. Process, 2015, 1, 0–4
[17] Parada, M., Vontobel, P., Rossi, R.M., Derome, D., Carmeliet, J., *Dynamic Wicking Process in Textiles*, In: Transp. Porous Media, 2017, 119, 611–632, https://doi.org/10.1007/s11242-017-0901-5
[18] Schledjewski, R., Blößl, Y., Neunkirchen, S., *Capillary Driven Saturation of Textile Reinforcing Structures Proposal for an Extension of Lucas-Washburn Equation*, In: Key Eng. Mater., 2022, 926 KEM, 1372–1378, https://doi.org/10.4028/p-7i6t7p
[19] Benltoufa, S., Fayala, F., Cheikhrouhou, M., Nasrallah, B., *Porosity determination of jersey structure*, In: Autex Res. J., 2007, 7, 63–69
[20] Benltoufa, S., Fayala, F., BenNasrallah, S., *Determination of yarn and fiber diameters after swelling using a capillary rise method*, In: J. Text. Inst., 2012, 103, 517–522, https://doi.org/10.1080/00405000.2011.589573
[21] Banuškevičiute, A., Adomavičiute, E., Milašius, R., *Investigation of water permeability of thermoplastic polyurethane (TPU) electrospun porous mat,* In: Medziagotyra, 2013, 19, https://doi.org/10.5755/j01.ms.19.2.4435
[22] Tsapko, Y., Bondarenko, O., Tsapko, O., *Research of Some Aspects of Water Permeability of Fire-Retardant Fabric for Tents*, In: Build. Constr. Theory Pract., 2022, 108-116, https://doi.org/10.32347/2522-4182.10.2022.108–116
[23] Patanaik, A., Anandjiwala, R., *Some Studies on Water Permeability of Nonwoven Fabrics,* In: Text. Res. J., 2009, 79, https://doi.org/10.1177/0040517508091313
[24] Atalie, D., Ferede, A., Rotich, G.K., *Effect of weft yarn twist level on mechanical and sensorial comfort of 100% woven cotton fabrics*, In: Fash. Text., 2019, 6, https://doi.org/10.1186/s40691-018-0169-6
[25] Benitoufa, S., Fayala, F., Bennasrallah, S., Cheikhrouhou, M., *Experimental device for fabric water permeability determination,* In: Melliand Int., 2007, 13, 140–143
[26] Benltoufa, S., Fayala, F., BenNasrallah, S., *Capillary Rise in Macro and Micro Pores of Jersey Knitting Structure*, In: J. Eng. Fiber Fabr., 2008, 3, 155892500800300, https://doi.org/10.1177/155892500800300305
[27] Heinisch, T., Těšinová, P., Pološčuková, L., *Moisture management for different air conditions*, In: Vlakna a Text., 2017, 24, 64–67
[28] Hussain, S., Glombikova, V., Havelka, A, Jamshaid, H., Batool, S.S., Khan, M.Z., *Moisture transport phenomena of functional underwears*, In: Vlakna a Text., 2017, 24, 59–66
[29] Masoodi, R., Pillai, K.M., *Darcy's law-based model for wicking in paper-like swelling porous media,* In: AIChE J., 2010, 56, 2257–2267, https://doi.org/10.1002/aic.12163
[30] Schwartz, A.M., *Capillarity: Theory and practice*, In: Ind. Eng. Chem., 1969, 61, 10–21, https://doi.org/10.1021/ie50709a004
[31] Chen, X., Kornev, K.G., Kamath, Y.K., Neimark, A.V., T*he Wicking Kinetics of Liquid Droplets into Yarns*, In: Text. Res. J., 2001, 71, 862–869, https://doi.org/10.1177/004051750107101003
[32] Mhetre, S., Parachuru, R., *The effect of fabric structure and yarn-to-yarn liquid migration on liquid transport in fabrics*, In: J. Text. Inst., 2010, 101, 621–626, https://doi.org/10.1080/00405000802696469

[33] Parkova, I., Ziemele, I., Vi, A., *Fabric Selection for Textile Moisture Sensor Design*, In: Mater. Sci. Text. Cloth. Technol., 2012, 1–3

[34] Alfaleh, A., Benltoufa, S., Fayala, F., *Evaporation coefficient determination during the capillary rise*, In: Text. Res. J., 2023, 93, 4191–4196, https://doi.org/10.1177/00405175231168425

[35] Benltoufa, S,. Oueslati, I., Boughattas, A., Fayala, F., *Saturation rate determination during ascendant, horizontal and descendant capillary rise using electrical resistivity,* In: Vlakna a Text., 2018, 25, 14–18

Authors:

SOFIEN BENLTOUFA[1], AYMAN ALFALEH[2]

[1]University of Monastir, National Engineering School of Monastir, Textile Engineering Department, 05000, Monastir, Tunisia

[2]College of Engineering and Computing, Mechanical and Industrial Engineering Department, Umm Al-Qura University, Al-Khalidiya District Al-Qunfudhah City 28821, Kingdom of Saudi Arabia
e-mail: affaleh@uqu.edu.sa

Corresponding author:

SOFIEN BENLTOUFA
e-mail: benltoufa@gmail.com